



Effects of rolling ball tool parameters on roughness, sheet thinning, and forming force generated during SPIF process

Lassaad Kilani¹ · Tarek Mabrouki¹ · Mahfoudh Ayadi^{1,2} · Hechmi Chermiti³ · Salim Belhadi⁴

Received: 17 October 2019 / Accepted: 30 December 2019 / Published online: 13 January 2020
© Springer-Verlag London Ltd., part of Springer Nature 2020

Abstract

Single-point incremental forming (SPIF) is a rising technology used shaping sheet-metals. The emergence of this manufacturing process is due to its capability to produce parts with complex shape at lower cost. The present contribution is focused on the presentation of a new designed rolling ball forming tool that can improve (SPIF) operations. For that, the effects of process working parameters on a set of process qualification criteria when forming of AA1050 aluminum alloy sheets is presented. Deep analyses treating impacts of tool step down, tool rolling ball diameter, and tool feed rate on the process responses such as forming axial forces, surface roughness, and sheet thinning are made. The analysis is based on statistical methodologies which made it possible to establish, using the multiple regression method, predictive analytical models for the different responses.

Keywords Incremental forming · ANOVA · RSM · Regression · Optimization · Design of experiments

Abbreviations

ANOVA	Analysis of variance
D	Rolling ball diameter (mm)
Df	Degrees of freedom
F	Tool feed rate (mm/min)
F _{avr}	Average axial forming force (N)
F _{max}	Maximal axial forming force (N)
F _z	Axial Forming force (N)
F-value	Fisher test value
ISF	Incremental sheet forming
MS	Mean squares
PC%	Percentage of contribution (%)
P value	Value of significance
RSM	Response surface methodology
R ²	Determination coefficient

R ² _{adjusted}	Adjusted determination coefficient
R ² _{predictif}	Predictive determination coefficient
R _a	Arithmetic mean roughness (μm)
R _z	Mean peak-to-valley height (μm)
R _t	Maximum profile height (μm)
SPIF	Single-point incremental forming
SS	Squared deviations
SS _D	Sum of squared deviations
SS _T	Total sum of squared deviations
ΔZ	Vertical step down (mm)
φ	Wall angle (degree)

✉ Tarek Mabrouki
tarek.mabrouki@enit.utm.tn

Lassaad Kilani
lasskilani@yahoo.fr

Mahfoudh Ayadi
mahfoudhayadi@gmail.com

Hechmi Chermiti
hechmi.chermiti@gmail.com

Salim Belhadi
belhadi23@yahoo.fr

¹ University of Tunis El Manar, ENIT, Applied Mechanics and Engineering Laboratory (LR-11-ES19), P.O. Box 37, Le Belvédère, 1002 Tunis, Tunisia

² University of Carthage, ENIB, Campus Universitaire Menzel Abderrahman, P.O. Box 66, Bizerte, 7035 Tunisia, Tunisia

³ University Campus Raccada, ISET de Kairouan, 3199 Kairouan, Tunisia

⁴ University of Guelma, May 8th 1945 Mechanics and Structures Laboratory LMS, P.O. Box 401, Guelma 24000, Algeria

1 Introduction

A new class of forming process known as incremental sheet forming (ISF) has emerged in the last few decades. From the beginning of this process with LESAK [1], various sectors of mechanical production have benefited from this process such as mentation, flexibility, and also employment. ISF is useful for rapid prototyping and limited batch [2] without a specific die. Emmens et al. [3] described the history of ISF in detail and focused mainly on technological development.

Following a predefined tool path controlled by a CNC machine, Iseki et al. [4] have developed the SPIF process which is based on the usage of a single tool to deform a metal sheet into a designed 3D shape. Matsubara [5] has proposed a two-point incremental forming (TPIF) process in which many types of tool were used to shape complex sheet metal parts. Jeswiet et al. [6] have studied the application of incremental CNC forming technology to an asymmetric shape.

This emerging technology is characterized by the fact that by means of the action of tool incremental movement, the workpiece is shaped by local plastic deformation. In addition to being adopted in a variety of industrial domains such as aeronautic, aerospace [7, 8], and automobiles industry [3], ISF has become increasingly important to produce different customized components for medical uses [9]. Moreover, it offers a valid manufacturing process to match the need of mass customization, which is regarded, among other processes, as the future of manufacturing [10].

Despite the spectacular progress that knows the ISF technology [11], many difficulties mastering this manufacturing process are still subject of studies [12]. These difficulties are caused by the high number of process parameters characterizing forming operations [13–14].

Indeed, it can be cited firstly, those concerning tooling used for forming (sheet fixing device and forming tool) [15–17]; secondly, other parameters related to material behavior and also to the complexity of the desired geometry [18]; and thirdly, the precision of the CNC machine to reproduce faithfully the programmed tool path [19] can be considered as another important parameter. It should be noted that the major problem that still posed up to now is how to define the appropriate tool strategy that must be adopted during the SPIF operation to obtain finished parts with optimum mechanical qualities and acceptable geometric tolerances [20] respecting imposed qualification criteria. This situation corresponds particularly to reduce shape deviation between programmed geometry and that corresponding to the manufactured parts.

To optimize ISF process, characterized by several responses, many methodologies have been developed aiming to predict responses associated to the forming process

operating variables. The most commonly used are response surface methodology (RSM), analysis of variance (ANOVA), and artificial neural networks (ANN) and fuzzy logic (FL).

Some researchers devote a great effort to develop a predictive model to understand the effect of process parameters on the evolution of forming force, surface roughness, and the deformed sheet thickness. Regarding forming force, Ambrogio et al. [21] have identified the impact of the tool diameter, the step down, the wall angle, and the sheet thickness on the tangential force when deforming by ISF three different materials. This provided that increasing each of those parameters will increase the force component. Aerens et al. [22] have proposed a new approach for the prediction of forming forces based on experimental results and finite element analysis. An approximation generalized formula is obtained allowing calculating the forming force component.

In the same way, Dwivedy et al. [23] have started the study to ascertain the nature of cutting forces expected during the SPIF process. They have analyzed the impact of process parameters on these forming forces. Based on experimental findings, pre-cited researchers have used ANOVA to elaborate the corresponded mathematical model. This result was presented in graphs allowing obtaining qualitative conclusions. Further, they proposed that it is possible to reduce forming forces with increased step down and large diameter tools. Other publications show opposing results concerning the evolution of axial forces as it was mentioned in the experimental and numerical study elaborated by Saidi et al. [24]. These authors have shown that the step-down displacement and the tool diameter have a great effect on the forming force evolution. It was clearly indicated from the obtained result that increasing these parameters yields an increase in the axial forming force. Furthermore, Dufloy et al. [25, 26] have adopted ANOVA analysis to calculate the statistical significance of the step down, the wall angle, the tool diameter, and the sheet thickness. The pre-cited analysis was performed according to the variation of vertical forming force. After, that the authors have developed a multilinear regression equation with those variables and conclude that if the vertical step size, tool diameter, wall angle, or sheet thickness is increased, the forces will increase accordingly.

The works related to predict surface roughness of parts produced by SPIF process can be shared into two classes. The first one contains experimentally designed models such as those developed by Liu et al. [27]. Built on the ANOVA analysis, these authors have expressed an empirical correlation performing surface roughness of the aluminum sheet metal parts according to ISF process control parameters. Also, in this first class, genetic programming, support vector regression, and artificial neural networks were used by Kurra et al.

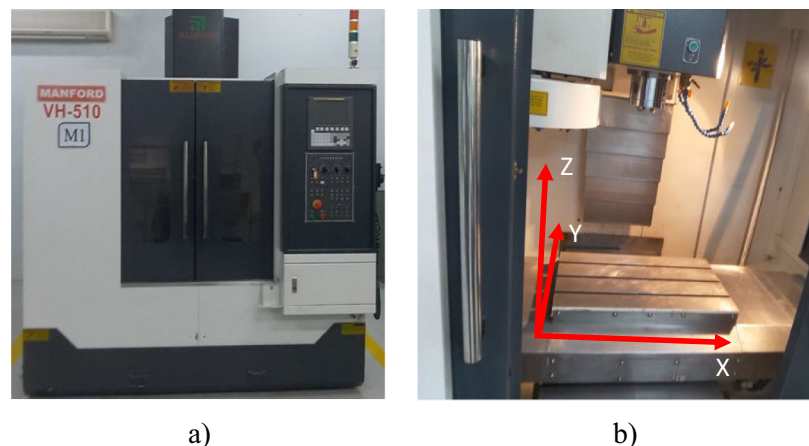
[28] to predict the surface roughness variation according to SPIF control parameters. The second class of studies is represented by analytical models such as that proposed by Durante et al. [29, 30] and highlighting the effect of wall angle and tool diameter on surface roughness. Concerning the thickness distribution, the same research was conducted to develop a mathematic model to predict the effect of the process parameter on the thinning ratio. Salem et al. [31] have described the thinning of deformed sheets as a result of progressive loading, the accumulated strains, and the uneven stresses generated by the contact with the tool. In addition, these researchers have developed a model dealing with the evolution of the thinning area, location of thinning, and its size. Also, Bahloul et al. [13] have used a statistical analysis such as ANOVA and a finite element simulation to comprehend the sheet thinning. They have proved that the wall angle and the initial sheet thickness have the significant effects on the sheet thinning rate. Li et al. [32] have found that the tool diameter and step down were nearly independent of the location of thickness. Nevertheless, the thickness thinning ratio increases as the tool diameter grows, continuously.

In the framework of the pre-cited research works, the present contribution deals with experimental study trying to identify the impact of the main ISF parameters on the quality of the manufactured components. An experimental design was conducted with a new invented roller ball tool, and the ball diameter is considered as one of the parameters in the forming process. An analysis ANOVA was carried out based on the experimental result to predict the forming force evolution, surface roughness variation, and sheet thinning.

2 Testing equipment and devices

This section presents the adopted experimental approach to study SPIF process. In the following, the CNC machine used,

Fig. 1 **a** MANFORD VH-510 CNC machining center. **b** A movable table of the CNC machine



the device designed for forming operations, the rolling ball tool geometry designed, the geometry, and the material of samples are presented.

2.1 Machine CNC

The forming tests were performed on a 5-axis CNC machining center (MANFORD VH-510 type) (Fig. 1a). It is equipped with a control system from Oi-MC control type of the FANUC series. In addition, this machine is provided with a movable table in the horizontal plane (Fig. 1b). These enable displacement cover range between 0 and 510 mm along first X axis and between 0 and 410 mm along second Y axis. The displacement along vertical Z axis is provided by spindle on which is fixed the forming tool. Its movement covers an interval varying between 0 and 460 mm.

2.2 Devices for clamping sheet samples

The specimen attachment device is designed in laboratory. It consists mainly in a blank holder, top thick plate, and support rigidly related by four columns (Fig. 2). Support is fixed on a CNC machine-movable table. Top thick plate and blank holder are used for clamping and fixing the sheet metal sample. Thus, the controlled displacements of the table are fully transmitted to the sheet sample.

The material selected for the sheet samples is AA1050-H24 aluminum alloy. The samples were cut by laser beam from 1-mm-thick sheet metal. The retained geometry of sheet sample is squared 200×200 mm; its central active area is also squared 100×100 mm (Fig. 3).

2.3 Forming tools

The forming tool used in this study is made on 304L stainless steel with a conical shape end (Fig. 4a). It has a hemispherical

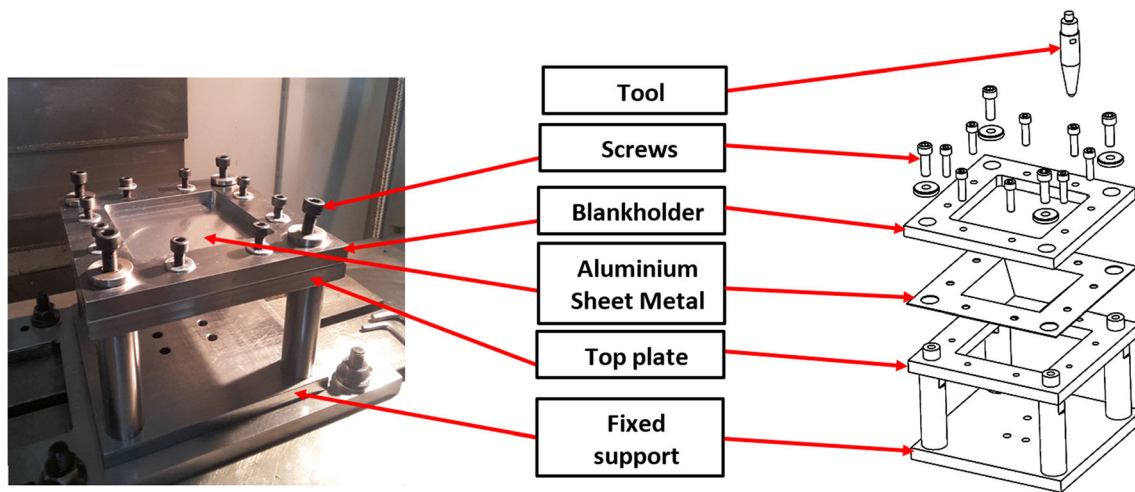


Fig. 2 A steel fixture mounted on the slide table of a CNC milling machine

cavity where a rolling ball is inserted (Fig. 4b). Used balls were extracted from SKF bearings and three ball diameters (D) were selected for the present experimental design (4.76 mm, 8.73 mm, and 12.70 mm). These SKF balls have a like-mirror surfaces which yield to reduce friction with blank, wear of contact surfaces, and deformed surface roughness, significantly.

It can be highlighted that, in this paper, a new tool design is proposed concerning the tool active part for SPIF as presented in (Fig. 4c, d). This new design has the following specifications:

- Roller is crowned by a set of balls arranged in annular form. This design helps centering the roller ball in its housing regarding the spindle axis.

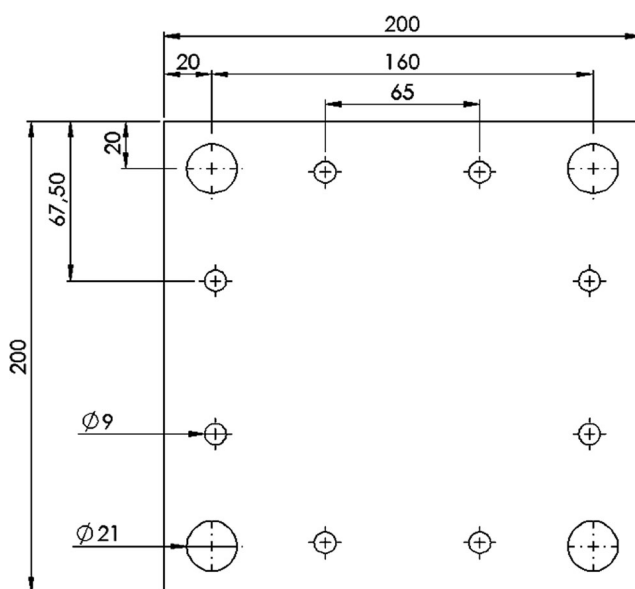


Fig. 3 Geometry of the tested sample (AA1050-H24 aluminum alloy)

- The ball housing of the roller ball is slightly bigger than the roller; this induces a reduction of peripheral ball housing/roller friction.
- The friction between the sheet and main roller ball is greater than that between the roller ball and balls arranged in annular form. This yields to improve the main roller ball rotation without sliding on the sheet.
- There is no need for any kind of lubricants.
- Also, it can be added a lubricating grease in balls arranged in annular form to reduce the main roller ball.
- The forming tool can be used without spindle rotation.
- The use of a rolling element supported by a ball ring protects the forming tool against wear.

Moreover, it can be underlined that among literature, a few authors have designed different housing parts for the roller ball. For example, the original idea to produce symmetric parts based on SPIF was patented by Leszak [1] who has designed a roller ball freely rotatable, fitted in a spherical concavity. Other authors [33–35] have proposed a conical housing for the roller ball. Matsubara [36] have patented a SPIF based on a roller ball housed in spherical concavity fitted with lubricating hole. Zhongyi [37] have designed a freely rotatable ball supported by a cap of small balls fitted in a spherical concavity. Lu et al. [38] have proposed a ball cap clamped by tool arm and fixed obliquely. Consequently, most of the designers of the SPIF tools have always tried to modify the active part of the tool, especially minimizing the contact and therefore the friction between the ball and its housing.

2.4 Forming axial force measurement method

Many SPIF process studies have shown the preponderance of the Z-axis force (along forming tool axis) compared to other ones. This preponderance becomes more significant with using roller ball tool, since rolling resistance is much less than

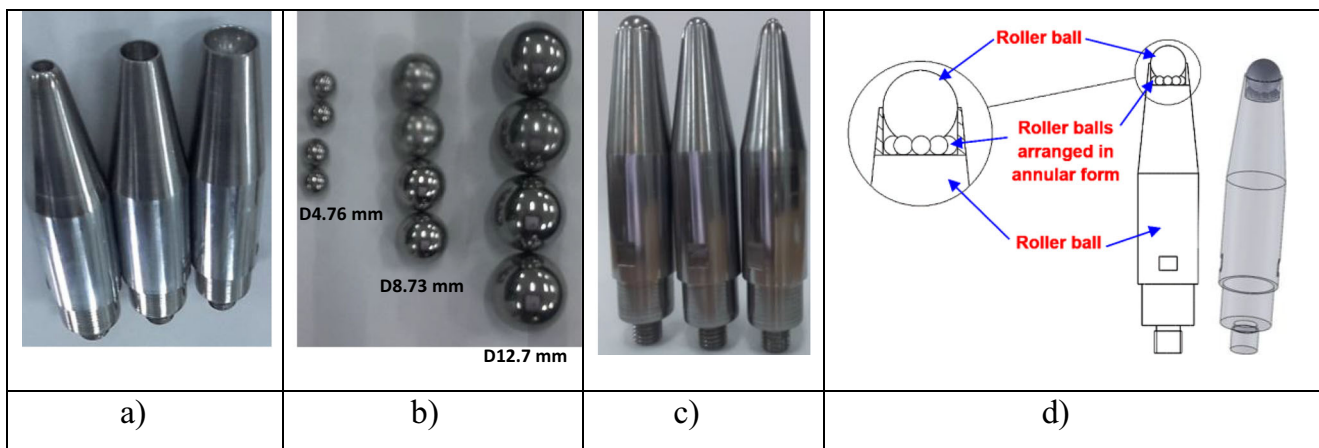


Fig. 4 Forming tools. **a** Tools without balls. **b** Balls. **c** Tools with balls. **d** Designed tool

resistance to sliding friction. As the CNC machine spindle produces mainly the axial tool displacement, a force sensor was exploited as an intermediate piece between forming tool and spindle (Fig. 5) to measure axial forming force. The load sensor used is a model marketed by METTLER TOLEDO. This sensor is able to measure compressive forces ranging from 0 to 500 daN, with a C3 precision class. It is wired to model DFWL of DINI ARGEO acquisition card. The registration and storage of data were carried out with the YAT Gamma 2" version 1.99.52 software (Fig. 5).

2.5 Measurements of deformed surface profile and roughness

To measure sheet thinning of pyramidal shape produced by forming operation, a coordinate measuring machine (CMM) type THOME MMT Rapid 544 was exploited.

This type of machine is used mainly to reduce the probability of error in measurement due to the absence of human interference. Also, all similar parts can be measured without any operator influence and with the same process. In addition, CMM was chosen for its effectiveness to not destroy the

dimensional inspection of samples which permit to re-use the forming piece.

The first step in this experiment was fixing the workpiece on a CMM jig using a special clamps kit (Fig. 6a). The second step was using the probe touch to get the coordinate of the profile from the front and back side and saving it as a form of a text file. The obtained data was transformed and generated through a CAD program called SolidWorks which was chosen to achieve authentic and speedy measurement results in drawing the two profiles of both sides. Finally, the two profiles were joined to compute minimum local thickness value.

In all of the experimental pieces, the local thickness value is taken equal to a distance separating parallel tangents to position curves taken on the upper and lower faces of the deformed shape, respectively, as shown in Fig. 6.

The finished surface roughness was measured through DIAVITE DH-7 tester possessing the following characteristics: 0.8 mm of cut-off, gauss sampling filter, and 0.5 mm/s measuring speed. This equipment is operated through the DIASOFT 7.4 software, according to the methodology recommended in SR ISO 4287-2001 (Fig. 7).

3 Experimental protocol and results

The present study mainly aims to evaluate effects and possible interactions of SPIF parameters such as tool step down increment, tool diameter and tool feed rate on sheet thinning, sheet surface roughness, forming force evolution, etc. In this section, the experimental approach and the main process responses according to the variation of working parameters are presented.

3.1 Experimental approach

During the adopted experimental design, shaped pyramidal samples were carried out. Indeed, this geometry helps

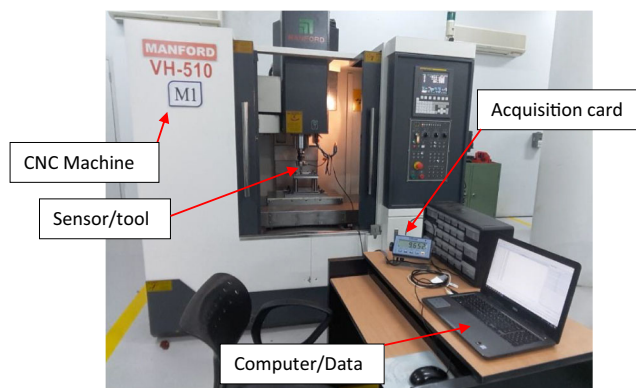
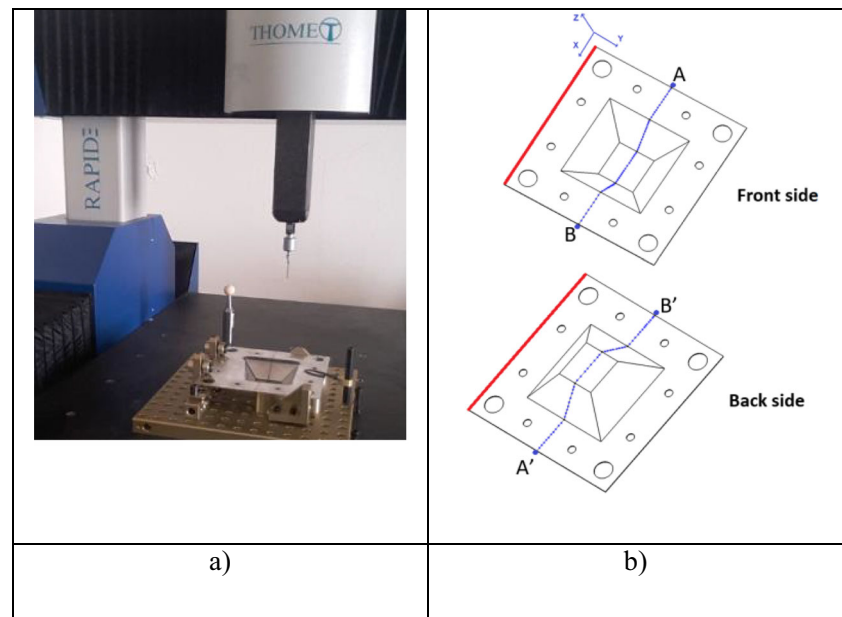


Fig. 5 SPIF experimental setup for measuring the forming axial force

Fig. 6 **a** THOME Rapid 544 coordinate measuring machine. **b** Front and back side probing paths



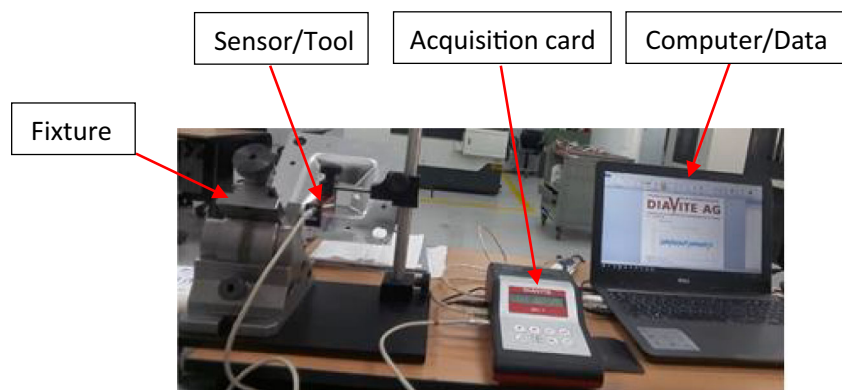
to control easily the forming operations such as measuring roughness, local sheet thinning, average thinning, and evaluation of dimensional deviations between finished parts and programmed analytical geometry etc. During SPIF process, the paths browsed by the forming tool/blank contact are generated by MasterCam software. These paths are parallel to each other and lie in horizontal planes, as it is shown in Figs. 8a). The distance separating two consecutive planes is fixed and is equal to increment step ΔZ (Fig. 8b) that is imposed by the user. Throughout the execution of the experimental design and for all samples achieved, pyramid wall inclination angle and maximum reached depth have been fixed respectively to 45° and 30 mm (Fig. 8b).

The responses of experimental tests concern the forming axial force magnitude, the sheet thickness distribution in the pyramidal geometry deformed region, and the roughness profile measured along the tool paths as shown in Fig. 9.

3.2 Forming axial force

Figure 10a shows a continuous record of forming force axial magnitude (F_z) obtained during the SPIF process. The evolution of F_z is characterized by stepped variations, where each stage indicates its magnitude growth during tool progression along a closed path. The maximum magnitude (Zoom in A) indicated a tool transition from one path to another; it is associated with the ΔZ step down axial displacement. The minimum force magnitude symbolizes that the forming tool returns to its initial contact point, with metal sheet, while remaining on the same path. These minimums can be correlated to restoring forces generated by sheet metal spring back. Between a maximum and a minimum, axial force fluctuations are observed, as shown in Fig. 10b (zoom in B, C, and D). These are explained by the displacement direction change of the tool which occurs at vertices (corners) of the same path.

Fig. 7 DIAVITE DH-7 tester possessing for measuring the surface roughness



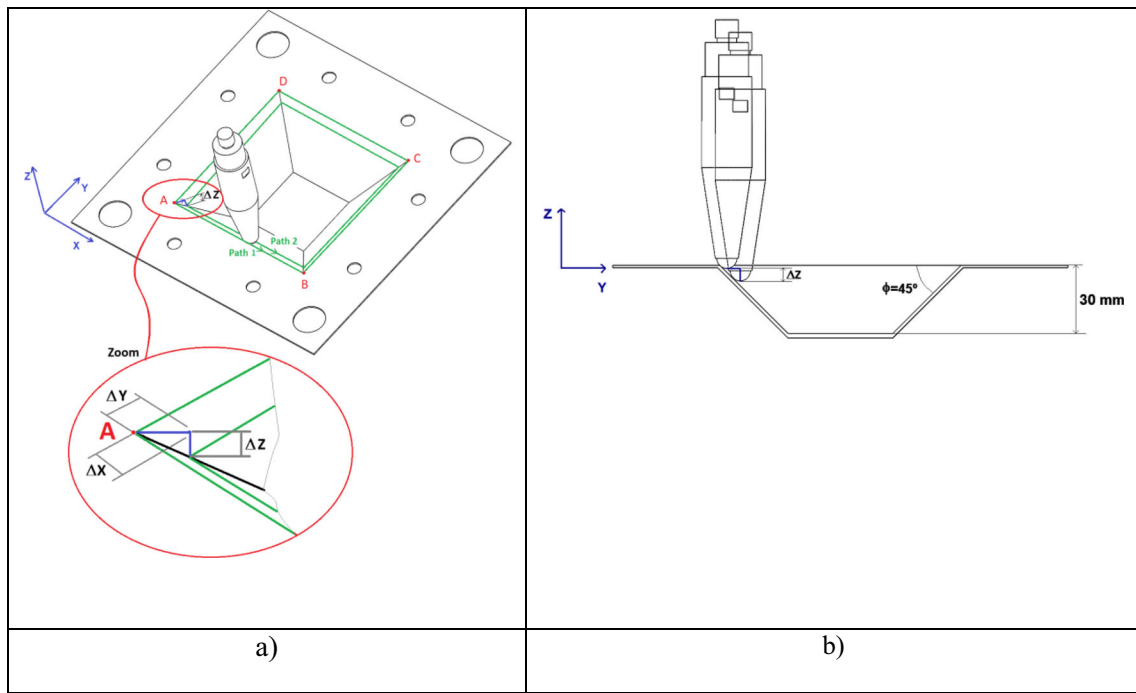


Fig. 8 a Tool path forming strategy of pyramidal samples. b Pyramid wall inclination angle and maximum reached depth.

The response, expressed in terms of axial force, highlights two operating regimes of SPIF process: an evolutionary stepped regime that spreads over the first eight paths performed by the tool, followed by a stability regime characterized by an asymptotic trend. In the following analysis, the magnitude levels of axial forming forces F_{avr} and F_{max} asymptotes will be highlighted.

3.3 Deformed sheet thickness distribution

Sheet thinning is the main problem of components manufactured by the ISF process. Indeed, when deformed part thickness becomes critical, the cracking becomes eminent,

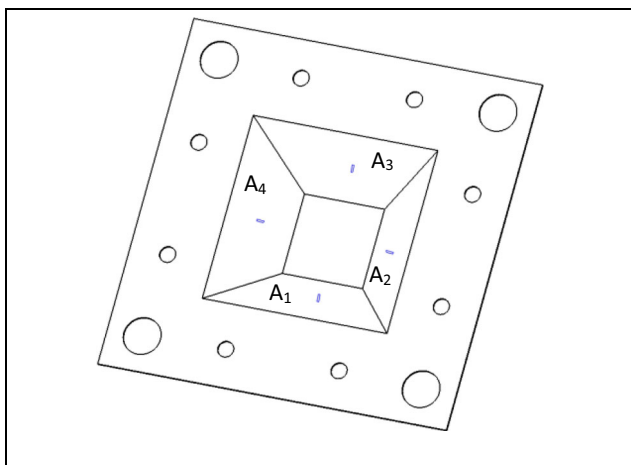


Fig. 9 The location of zone where roughness has been measured

and mechanical resistance of component undergoes degradation which may cause its rejection. In this study, the thickness distribution was deduced from the inner and outer profiles measured on the same cross section. These sections were occupied symmetry planes of produced samples, as shown in Fig. 6b.

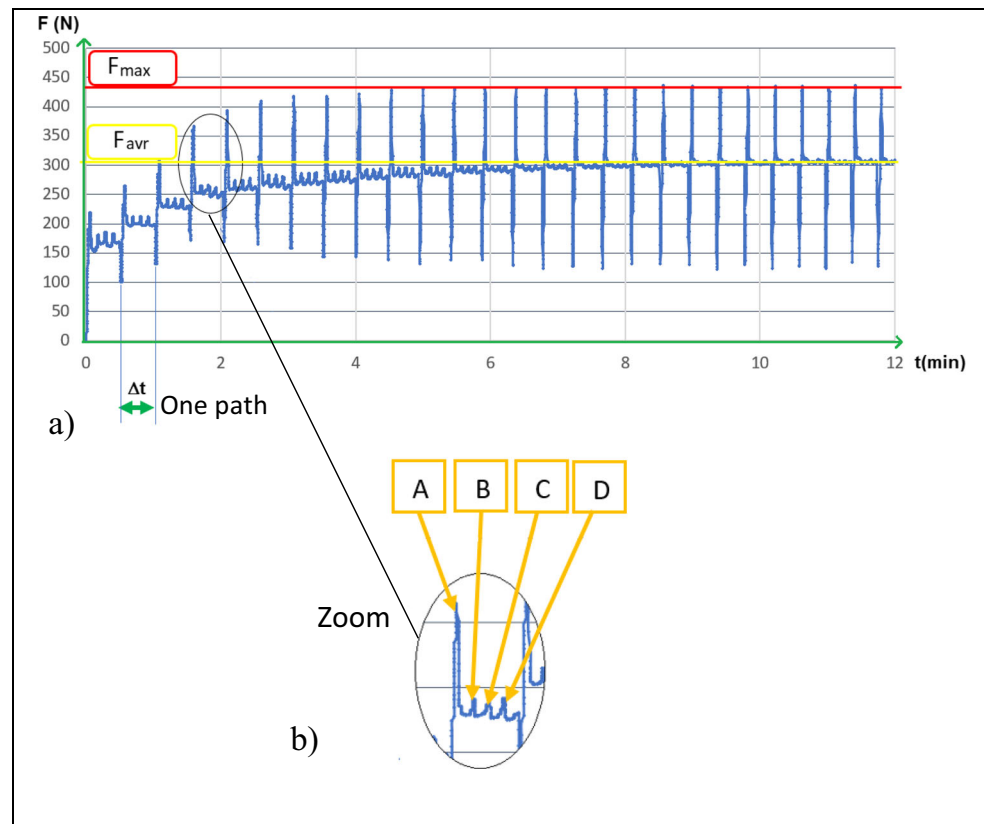
3.4 Surface roughness generated by forming

To characterize the surface state of parts obtained by incremental forming, three types of roughness measurements were performed, according to ISO4287 standard. The first one is the arithmetical mean roughness value R_a , the second one is total height of the roughness profile R_t , and the third one is the mean roughness depth R_z . Based on Fig. 11, it is possible to compare roughness profiles obtained successively with a rolling ball and a hemispherical tool with the same diameter. The obtained results show the interest of rolling ball tools in improving surface integrity expressed in terms of roughness. Table 1 shows the variation ranges of the different roughness that characterize the quality of the part surfaces obtained by incremental forming with of the pre-cited tools.

4 Experimental design and collected results

The objective of this section is to establish correlations able to predict responses, related to the forming process, with an acceptable confidence level when the SPIF control parameters evolve within well-defined intervals. The control parameters

Fig. 10 **a** Forming axial force evolution during SPIF process ($D = 4.76$ mm, $\Delta Z = 0.6$ mm, $V = 900$ mm/min). **b** Axial force fluctuation in the 4th step down



(factors) for the present study included rolling ball diameter (D), tool feed rate (F), and vertical step down (ΔZ). As indicated in Table 2, three levels for each factor selected were fixed. To limit the number of forming tests, a factorial design executed in 27 tests was adopted.

The main responses associated to these factors are average and maximum forming axial force obtained after force stabilization (F_{avr} , F_{max}), surface roughness swept by the tool/blank contact (R_a , R_z , and R_t), and minimum thickness Th_{min} measured at the flat parts of the stretched pyramid.

Moreover, the same operating procedure was maintained for all tests by applying total locking of the spindle where the rolling ball tool is mounted. In addition, only the table of the CNC machine, where forming pilot is fixed, is controlled in speed and displacement. To avoid ball wear, a new roller ball has been used in each test. Adding to changing the rolling element after each forming process, a check of the surface condition of the removed ball is carried out. Table 3 summarizes all the data and experimental results of the 27 tests performed.

4.1 Mathematical analysis of test results

Mathematical analysis consists in developing models able to predict the responses corresponding to a predefined operating mode. In this section, the RSM methodology was adopted to

optimize the SPIF incremental forming factors (D , ΔZ , F) associated with the desired responses such as forming forces, roughness parameters, and sheet thinning. For the present analysis, the responses are represented analytically by quadratic forms as expressed by Eq. 1:

$$Y = C_0 + C_1D + C_2\Delta Z + C_3F + C_{11}D^2 + C_{22}\Delta Z^2 + C_{33}F^2 + C_{12}D.\Delta Z + C_{13}D.F + C_{23}\Delta Z.F + \varepsilon \quad (1)$$

where

Y : response estimated by the model

C_0 : average value of the response

C_1 , C_2 , and C_3 : coefficients representing linear effects

C_{11} , C_{22} , and C_{33} : coefficients associated with quadratic effects

C_{12} , C_{13} , and C_{23} : coefficients representing the double interaction effects

ε : difference between the observed value and the calculated one

4.2 Coefficients of mathematical models

The coefficients of the coded models were obtained by multiple regression's technique using Design Expert software. Table 4 summarizes results of coefficient calculations made

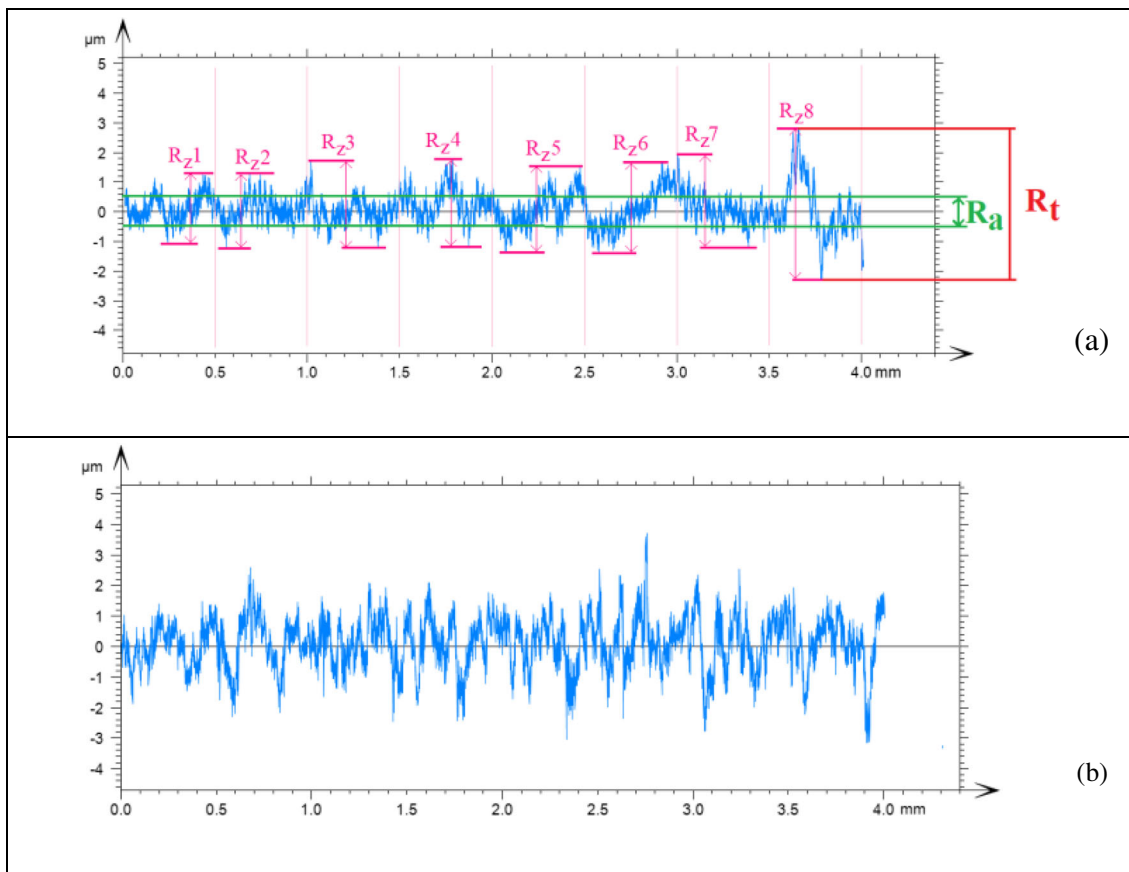


Fig. 11 Profilometer trace of surface roughness ($D = 12.7$ mm, $Z = 0.2$ mm and $F = 900$ mm/min). **a** The new design of roller ball tools. **b** The rigid hemispherical head tool

corresponding to a first step taking into account different effects related to linear, quadratic, and double interactions terms.

4.3 Statistical analysis of results

The objective of statistical analysis is to make a judgment on results obtained through an

- Assessment of the quality associated to models' coefficient estimation (ANOVA)
- Estimation of model descriptive quality, in the experimental domain using the determination coefficients R^2 , $R^2_{\text{predictif}}$ and R^2_{adjusted}

Table 1 Range of the roughness ($D = 12.7$ mm, $Z = 0.2$ mm, and $F = 900$ mm/min)

	Rolling ball tools			Tools with hemispherical head		
	R_a (μm)	R_z (μm)	R_t (μm)	R_a (μm)	R_z (μm)	R_t (μm)
Min	0.53	3.14	5.08	0.65	3.92	6.85
Max	0.637	3.65	6.97	1.27	6.44	11.45

- Estimation of model validity with residuals reflecting differences between measured values and calculated ones

The analysis of variance (ANOVA) allows identification of the forming factors, retained in the experiments design, affecting responses, significantly. The regression models are developed with the Design Expert software. The results obtained by applying the ANOVA led to the results presented successively in Tables 5, 6, 7, 8, 9, and 10.

The objective of the analysis is to establish reliable models able to predict responses corresponding to a predefined configuration of the SPIF process parameters. The analysis conducted is obtained with 95% of confidence level. The tables successively show sum of the squared deviations (SS), degree of freedom (Df), mean squares (MS), Fisher test value (F-

Table 2 Range of the investigate process parameters

Factors	Unit	Symbol	Level		
Tool rolling ball	mm	D	4.76	8.73	12.70
Step down	mm	ΔZ	0.2	0.6	1.0
Feed rate	mm/min	F	300	900	1500

Table 3 Experimental results of performed tests

Test	Factors			Responses					
	D (mm)	ΔZ (mm)	F (mm/min)	R_a (μm)	R_z (μm)	R_t (μm)	F_{avr} (N)	F_{max} (N)	Th_{min} (mm)
1	4.76	0.2	300	0.989	6.515	11.74	259	278	0.63
2	4.76	0.2	900	0.934	6.048	10.52	263	281	0.64
3	4.76	0.2	1500	1.029	6.025	11.97	269	284	0.64
4	4.76	0.6	300	3.63	15.7	19.28	309	452	0.66
5	4.76	0.6	900	3.173	13.73	18.38	309	440	0.65
6	4.76	0.6	1500	2.87	12.43	16.08	312	448	0.65
7	4.76	1.0	300	3.563	15.73	25.33	323	562	0.66
8	4.76	1.0	900	3.535	15.45	25.95	332	567	0.68
9	4.76	1.0	1500	3.64	17.33	26.13	335	574	0.67
10	8.73	0.2	300	0.719	4.195	7.488	318	375	0.70
11	8.73	0.2	900	0.799	4.818	7.988	323	377	0.72
12	8.73	0.2	1500	1.054	5.73	7.76	321	377	0.71
13	8.73	0.6	300	2.358	10.81	15.08	362	604	0.70
14	8.73	0.6	900	2.303	11.13	15.13	371	606	0.72
15	8.73	0.6	1500	2.498	11.4	14.23	365	615	0.71
16	8.73	1.0	300	1.498	7.208	14.65	381	714	0.71
17	8.73	1.0	900	1.738	8.34	14.88	391	732	0.70
18	8.73	1.0	1500	1.705	8.263	16.18	394	730	0.69
19	12.70	0.2	300	0.614	3.548	6.205	366	475	0.72
20	12.70	0.2	900	0.587	3.46	6.635	370	466	0.71
21	12.70	0.2	1500	0.649	3.735	6.908	373	483	0.71
22	12.70	0.6	300	1.348	6.553	8.273	414	741	0.73
23	12.70	0.6	900	1.448	6.763	9.015	425	749	0.76
24	12.70	0.6	1500	1.463	6.978	9.493	430	758	0.75
25	12.70	1.0	300	1.1	6.085	11.28	435	891	0.73
26	12.70	1.0	900	1.092	6.118	10.98	445	900	0.75
27	12.70	1.0	1500	1.092	5.533	11.83	459	918	0.74

value), value of significance (P value), and percentage of contribution (%) of each typical terms. In this analysis, when P value is less than 0.05, this indicates that the elaborated analytical models are adequate and the terms are having a significant effect on responses.

Analysis by the ANOVA method (Tables 5 and 11) shows that the rolling ball diameter, D , is the main factor affecting the axial component of the average forming force F_{avr} with a contribution rate of about 70%. In the same way, the increment ΔZ is the second most important factor with a

Table 4 Coefficients of the coded models in first step

Coefficients	F_{avr} (N)	F_{max} (N)	R_a (μm)	R_z (μm)	R_t (μm)	Th_{min} (mm)
C0	368.44	+ 599.59	+ 2.19	+ 10.02	+ 13.13	+ 0.7178
C1	55.89	+ 138.61	- 0.7762	- 3.34	- 4.71	+ 0.0400
C2	35.17	+ 177.33	+ 0.6437	+ 2.55	+ 4.44	+ 0.0083
C3	5.06	+ 5.28	+ 0.0101	+ 0.0600	+ 0.0693	+ 0.0017
C12	2.58	+ 35.42	- 0.5292	- 1.91	- 2.40	- 0.0017
C13	1.83	+ 3.17	+ 0.0653	+ 0.1854	+ 0.3871	+ 0.0008
C23	2.42	+ 3.25	- 0.0111	+ 0.0725	+ 0.1394	- 0.0008
C11	- 1.33	+ 0.3889	+ 0.1895	+ 0.7746	+ 1.07	- 0.0133
C22	- 13.17	- 46.78	- 0.8800	- 3.16	- 0.8599	- 0.0083
C33	- 1.83	+ 2.39	+ 0.0334	+ 0.1142	+ 0.0526	- 0.0083

Table 5 ANOVA results for average forming axial force F_{avr}

Source	SS	Df	MS	F-value	P value	PC%
Model	80,206.28	9	8911.81	910.52	< 0.0001	99.79
D	56,224.22	1	56,224.22	5744.44	< 0.0001	69.95
ΔZ	22,260.5	1	22,260.50	2274.36	< 0.0001	27.70
F	460.06	1	460.06	47	< 0.0001	0.57
$D \times \Delta Z$	80.08	1	80.08	8.18	0.0108	0.10
$D \times F$	40.33	1	40.33	4.12	0.0583	0.05
$\Delta Z \times F$	70.08	1	70.08	7.16	0.016	0.09
D^2	10.67	1	10.67	1.09	0.3111	0.01
ΔZ^2	1040.17	1	1040.17	106.27	< 0.0001	1.29
F^2	20.17	1	20.17	2.06	0.1693	0.03
Residual	166.39	17	9.79			0.21
Cor Total	80,372.67	26				100

contribution rate of about 35%. The factors having the lowest contribution rates are F, $D \times \Delta Z$, $\Delta Z \times F$, and ΔZ^2 with rates evolving between 0.09 and 1.30%.

Table 6 presents results coming from ANOVA methodology applied to maximal forming force. These results indicate that ΔZ and ball diameter D are the factors having the most important effects on F_{max} level with contribution rate of about 60 and 37%, respectively. Interactions and quadratic terms occur weakly across $D \times \Delta Z$ and ΔZ^2 with contributions below 1.6%.

From the analysis of Tables 7, 8, and 9, the incremental forming parameters show a significant effect on responses expressed by surfaces roughness R_a , R_z , and R_t . The results based on ANOVA show that the factors with the greatest impact, on the three types of surface roughness, are mainly the diameter D of the rolling ball, integrated into the forming tool, and the step down ΔZ with a

Table 6 ANOVA results for the forming maximal axial force F_{max}

Source	SS	Df	MS	F-value	P value	PC%
Model	9.41E+05	9	1.05E+05	811.56	< 0.0001	99.77
D	3.46E+05	1	3.46E+05	2684.81	< 0.0001	36.67
ΔZ	5.66E+05	1	5.66E+05	4394.39	< 0.0001	60.02
F	501.39	1	501.39	3.89	0.065	0.05
$D \times \Delta Z$	15,052.08	1	15,052.08	116.85	< 0.0001	1.60
$D \times F$	120.33	1	120.33	0.9342	0.3473	0.01
$\Delta Z \times F$	126.75	1	126.75	0.984	0.3351	0.01
D^2	0.9074	1	0.9074	0.007	0.9341	0.00
ΔZ^2	13,128.96	1	13,128.96	101.92	< 0.0001	1.39
F^2	34.24	1	34.24	0.2658	0.6128	0.00
Residual	2189.80	17	128.81			0.23
Cor Total	9.43E+05	26				100

Table 7 ANOVA results for surface roughness R_a

Source	SS	Df	MS	F-value	P value	PC%
Model	26.59	9	2.95	39.78	< 0.0001	95.48
D	10.85	1	10.85	146.05	< 0.0001	38.96
ΔZ	7.46	1	7.46	100.44	< 0.0001	26.79
F	0.0018	1	0.0018	0.0246	0.8771	0.01
$D \times \Delta Z$	3.36	1	3.36	45.26	< 0.0001	12.06
$D \times F$	0.0512	1	0.0512	0.6897	0.4178	0.18
$\Delta Z \times F$	0.0015	1	0.0015	0.02	0.8892	0.01
D^2	0.2155	1	0.2155	2.9	0.1067	0.77
ΔZ^2	4.65	1	4.65	62.57	< 0.0001	16.70
F^2	0.0067	1	0.0067	0.0899	0.7679	0.02
Residual	1.26	17	0.0743			4.52
Cor Total	27.85	26				100.00

contribution rate evaluating between 26 and 46%. The analysis shows that only $D \times \Delta Z$ interaction has an influence on the roughness parameters within contribution limits between 8 and 12%. It is also underlined that the only quadratic term that has an impact on surface roughness is ΔZ^2 . This term affects only parameters R_a and R_z responses with contribution levels of 13 and 17%, respectively.

Table 10 summarizes the ANOVA results corresponding to the minimum thicknesses measured (Th_{min}). These findings indicate that the largest thinning is strongly influenced by the rolling ball diameter D and its square D^2 , and their respective contribution rates are 81.59% and 3.12%. Nevertheless, the step down ΔZ contributes slightly to the sheet thinning with a contribution rate of about 3.68%.

Table 8 ANOVA result for surface roughness R_z

Source	SS	Df	MS	F-value	P value	PC%
Model	426.33	9	47.37	29.95	< 0.0001	94.07
D	201.12	1	201.12	127.15	< 0.0001	44.38
ΔZ	117.42	1	117.42	74.23	< 0.0001	25.91
F	0.0648	1	0.0648	0.041	0.842	0.01
$D \times \Delta Z$	43.78	1	43.78	27.68	< 0.0001	9.66
$D \times F$	0.4126	1	0.4126	0.2608	0.6161	0.09
$\Delta Z \times F$	0.0631	1	0.0631	0.0399	0.8441	0.01
D^2	3.6	1	3.6	2.28	0.1498	0.79
ΔZ^2	59.8	1	59.8	37.81	< 0.0001	13.19
F^2	0.0782	1	0.0782	0.0494	0.8267	0.02
Residual	26.89	17	1.58			5.93
Cor Total	453.22	26				100

Table 9 ANOVA Result for surface roughness R_t

Source	SS	Df	SM	F-value	P value	PC%
Model	837.04	9	93	50.65	< 0.0001	96.40
D	399.01	1	399.01	217.31	< 0.0001	45.96
ΔZ	355.27	1	355.27	193.49	< 0.0001	40.92
F	0.0865	1	0.0865	0.0471	0.8308	0.01
$D \times \Delta Z$	69.35	1	69.35	37.77	< 0.0001	7.99
$D \times F$	1.8	1	1.8	0.9792	0.3363	0.21
$\Delta Z \times F$	0.2331	1	0.2331	0.127	0.726	0.03
D^2	6.85	1	6.85	3.73	0.0703	0.79
ΔZ^2	4.44	1	4.44	2.42	0.1385	0.51
F^2	0.0166	1	0.0166	0.0091	0.9253	0.00
Residual	31.21	17	1.84			3.59
Cor Total	868.26	26				100

Table 10 ANOVA results for minimal thickness Th_{min}

Source	SS	Df	MS	F-value	P value	PC%
Model	0.032	9	0.0036	18.82	< 0.0001	90.65
D	0.0288	1	0.0288	152.21	< 0.0001	81.59
ΔZ	0.0013	1	0.0013	6.61	0.0199	3.68
F	0.0001	1	0.0001	0.2642	0.6138	0.28
$D \times \Delta Z$	0	1	0	0.1762	0.6799	0.00
$D \times F$	8.33E-06	1	8.33E-06	0.044	0.8363	0.02
$\Delta Z \times F$	8.33E-06	1	8.33E-06	0.044	0.8363	0.02
D^2	0.0011	1	0.0011	5.64	0.0296	3.12
ΔZ^2	0.0004	1	0.0004	2.2	0.1561	1.13
F^2	0.0004	1	0.0004	2.2	0.1561	1.13
Residual	0.0032	17	0.0002			9.07
Cor Total	0.0353	26				100.00

5 Multiple regression models

The ANOVA analysis conducted previously led to the identification of the insignificant coefficients needed for the elaboration of mathematical models. This section presents the adopted approach helping to determine the most relevant regression models using a step-by-step top-down elimination method. The selected method uses a complete model (Table 4) to extract coefficients one by one starting with the one with the highest probability (P value > 0.05). At each iteration, the analysis of variance makes it possible to identify the model term whose impact, on the response, is the least important. In fact, this one corresponds to the highest P value.

5.1 Regression results

At each iteration of analysis, the model coefficients are identified. To this identification, the standard deviation and the determination coefficients (R^2 , $R^2_{adjusted}$, $R^2_{predictive}$) are associated. Tables 11 and 12 summarize the results of the different calculation steps for the particular case of the average and maximal forming forces (F_{avr} and F_{max}).

By proceeding in the same way for the other responses, the final predictive models of surface roughness and sheet thinning could be established. Table 13 presents the coefficients of the selected models, the responses concerned by these models, and the number of iterations performed. The results of the calculations show that the predictive models of the forming forces F_{avr} and F_{max} are obtained with determination coefficients evolving between 0.995 and 0.997, respectively. This makes it possible to qualify these models as accurate ones. The determination coefficients associated to the surface roughness models range from 0.868 to 0.948; those associated to sheet thinning vary between 0.837 and 0.882. These

coefficients indicate that the accuracy of the predictions of R_a , R_z , and R_t and the accuracy of the Th_{min} sheet thinning will be less important than those of the forming forces.

5.2 Predictive correlations

The predictive correlations between incremental forming parameters and performed measurements were modeled by quadratic regression. These correlations are presented with their coefficients of determination R^2 in Table 14. The proposed equations are useful for predicting responses, expressed by F_{avr} , F_{max} , R_a , R_z , R_t and Th_{min} , based on the actual factor (operating parameters) of the incremental forming process.

Figures 12, 13, and 16a) present the model predictions to the function of the experimental results obtained successively in the cases of axial forming forces, surface roughness, and the minimal sheet thinning. All the 27 points marked, on each graph, can be classified according to their location in relation to the first bisector. The first class consists of the points located on the bisector; they indicate identical predictions or sufficiently close to the experimental results. The second one brings together the points located below the bisector, showing forecasts overestimating the experiment results. Finally, the third class is composed of the points located above. This set indicates underestimating the values obtained experimentally.

To better visualize the quality of correlations, the relative fluctuations of the predictions were compared to experimental measurements obtained for all the 27 trials. For each test, the relative fluctuation of a response is calculated using the relationship expressed by Eq. 8:

$$FL(\%) = 100 \times \left(\frac{\text{experimental result} - \text{predicted result}}{\text{experimental result}} \right) \quad (8)$$

Table 11 Coefficients of coded models at different iterations (case of the average forming force: F_{avr})

	Iteration 1		Iteration 2		Iteration 3		Iteration 4	
	Coef	P value	Coef	P value	Coef	P value	Coef	P value
Cons	+ 368.44		+ 367.56		+ 366.33		+ 366.33	
D	+ 55.89	$< 10^{-4}$	+ 55.89	$< 10^{-4}$	+ 55.89	$< 10^{-4}$	+ 55.89	$< 10^{-4}$
ΔZ	+ 35.17	$< 10^{-4}$	+ 35.17	$< 10^{-4}$	+ 35.17	$< 10^{-4}$	+ 35.17	$< 10^{-4}$
F	+ 5.06	$< 10^{-4}$	+ 5.06	$< 10^{-4}$	+ 5.06	< 0.0001	+ 5.06	$< 10^{-4}$
$D \times \Delta Z$	+ 2.58	0.0108	+ 2.58	0.0106	+ 2.58	0.0120	+ 2.58	0.0173
$D \times F$	+ 1.83	0.0583	+ 1.83	0.0580	+ 1.83	0.0634		
$\Delta Z \times F$	+ 2.42	0.0160	+ 2.42	0.0156	+ 2.42	0.0176	+ 2.42	0.0247
D^2	- 1.33	0.3111						
ΔZ^2	- 13.17	$< 10^{-4}$	- 13.17	$< 10^{-4}$	- 13.17	$< 10^{-4}$	- 13.17	$< 10^{-4}$
F^2	- 1.83	0.1693	- 1.83	0.1693				
S	3.13		3.14		3.22		3.45	
R^2	0.9979		0.9978		0.9975		0.9970	
R^2 adj	0.9968		0.9968		0.9966		0.9962	
R^2 pred	0.9943		0.9947		0.9948		0.9946	

Figures 14, 15, and 16b summarize the fluctuations for different responses collected from the test campaigns that were conducted. The diagrams show that the smallest fluctuations correspond to the axial force with its two magnitudes: average and maximal ones. The relative fluctuations, for the average force, are varying in the range of $[-1.75\%; 1.54\%]$. Those corresponding to the maximum force are in the range of $[-5.20\%; 3.47\%]$.

The fluctuations (%) associated to surface roughness R_a , R_z , and R_t evolve in the intervals: $[-40.61; 27.16]$, $[-38.81; 22.31]$, and $[-21.16; 12.01]$, respectively. As for the

maximum sheet thinning of the deformed sheet, it fluctuates between $- 5.19$ and 3.47 .

6 Effect of incremental forming parameters on surfaces responses

The effects of incremental forming parameters (D, F, and ΔZ) on responses of deformed surfaces such as axial forming force, surface roughness, and thinning are discussed in this

Table 12 Coefficients of coded models at different iterations. (Case of the average forming force: F_{max})

	Iteration 1		Iteration 2		Iteration 3		Iteration 4		Iteration 5		Iteration 6	
	Coef	P value	Coef	P value	Coef	Coef	Coef	P value	Coef	P value	Coef	P value
Cons	599.6		+ 599.85		+ 601.44		+ 601.44		+ 601.44		+ 601.44	
D	138.61	$< 10^{-4}$	+ 138.61	$< 10^{-4}$	+ 138.61	$< 10^{-4}$	+ 138.61	$< 10^{-4}$	+ 138.61	$< 10^{-4}$	+ 138.61	$< 10^{-4}$
ΔZ	177.33	$< 10^{-4}$	+ 177.33	$< 10^{-4}$	+ 177.33	$< 10^{-4}$	+ 177.33	$< 10^{-4}$	+ 177.33	$< 10^{-4}$	+ 177.33	$< 10^{-4}$
F	5.28	0.0650	+ 5.28	0.0574	+ 5.28	0.0574	+ 5.28	0.0518	+ 5.28	0.0516		
$D \times \Delta Z$	35.42	$< 10^{-4}$	+ 35.42	$< 10^{-4}$	+ 35.42	$< 10^{-4}$	+ 35.42	$< 10^{-4}$	+ 35.42	$< 10^{-4}$	+ 35.42	$< 10^{-4}$
$D \times F$	3.17	0.3473	+ 3.17	0.3332	+ 3.17	0.3332						
$\Delta Z \times F$	3.25	0.3351	+ 3.25	0.3210	+ 3.25	0.3210	+ 3.25	0.3109				
D^2	+ 0.3889	0.9341										
ΔZ^2	- 46.78	$< 10^{-4}$	- 46.78	$< 10^{-4}$	- 46.78	$< 10^{-4}$	- 46.78	$< 10^{-4}$	- 46.78	$< 10^{-4}$	- 46.78	$< 10^{-4}$
F^2	+ 2.39	0.6128	+ 2.39	0.6023								
S	11.35		11.03		10.82		10.83		10.85		11.63	
R^2	0.9977		0.9977		0.9976		0.9975		0.9974		0.9968	
R^2 adj	0.9964		0.9966		0.9968		0.9968		0.9968		0.9963	
R^2 pred	0.9944		0.9948		0.9952		0.9956		0.9956		0.9951	

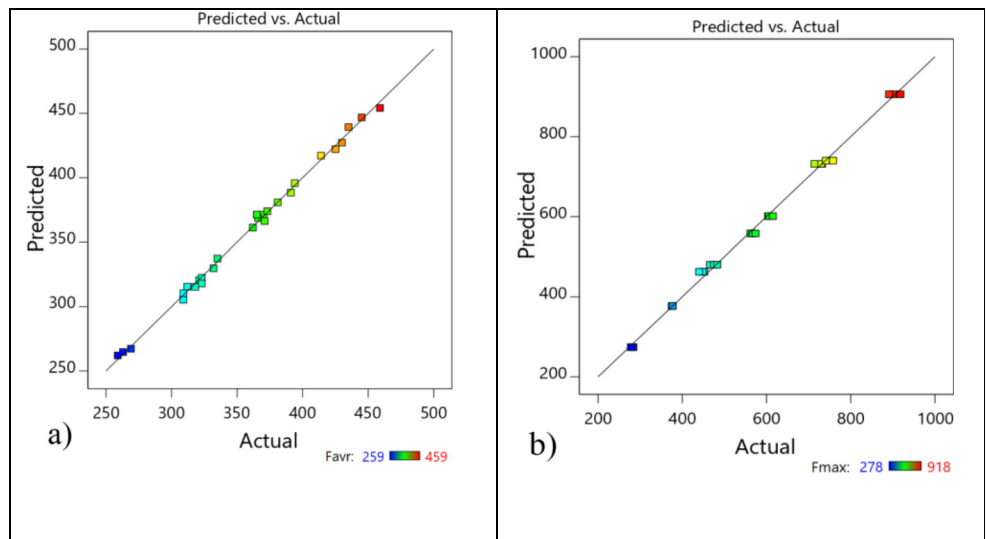
Table 13 Coefficients of the coded models obtained at the last iteration of surface roughness and thinning parameters

Parameter	R_a		R_z		R_t		Th_{min}	
	Coef	<i>P</i> value	Coef	<i>P</i> value	Coef	<i>P</i> value	Coef	<i>P</i> value
Iter. number	6		6		7		7	
Cons	2.34		10.61		13.31		0.7067	
D	-0.7762	$< 10^{-4}$	-3.34	$< 10^{-4}$	-4.71	$< 10^{-4}$	0.0400	$< 10^{-4}$
ΔZ	0.6437	$< 10^{-4}$	+2.55	$< 10^{-4}$	4.44	$< 10^{-4}$	0.0083	0.0149
F								
$D \times \Delta Z$	-0.5292	$< 10^{-4}$	-1.91	$< 10^{-4}$	-2.40	$< 10^{-4}$		
$D \times F$								
$\Delta Z \times F$								
D^2							-0.0133	0.0232
ΔZ^2	-0.8800	$< 10^{-4}$	-3.16	$< 10^{-4}$				
F^2								
S	0.2645		1.22		1.39		0.0134	
R^2	0.9447		0.9405		0.9486		0.8823	
R^2_{adj}	0.9347		0.9141		0.9419		0.8670	
R^2_{pred}	0.9206		0.8683		0.9351		0.8370	

Table 14 Predictive regressions of forming forces, surface roughness, and thinning versus actual operating parameters

Predictive correlations	R^2	Equation number
$F_{avr} = 167.43 + 13.10D + 163.40\Delta Z + 0.0024F + 1.63D \times \Delta Z + 0.01\Delta Z \times F - 82.29\Delta Z^2$	0.997	(2)
$F_{max} = 42.21 + 21.53D + 599.46\Delta Z + 22.30D \times \Delta Z - 292.36\Delta Z^2$	0.997	(3)
$R_a = -0.64 + 0.0045D + 11.12\Delta Z - 0.33D - 5.50\Delta Z^2$	0.941	(4)
$R_z = 0.73 - 0.12D + 40.56\Delta Z - 1.20D \times \Delta Z - 19.73\Delta Z^2$	0.941	(5)
$R_t = 9.07 - 0.28D + 24.32\Delta Z - 1.51D \times \Delta Z$	0.949	(6)
$Th_{min} = 0.542 + 0.025D + 0.021\Delta Z - 0.00085D^2$	0.882	(7)

Fig. 12 Regression predictions versus experimental measurements. **a** Average axial force F_{avr} . **b** Maximal axial force F_{max}



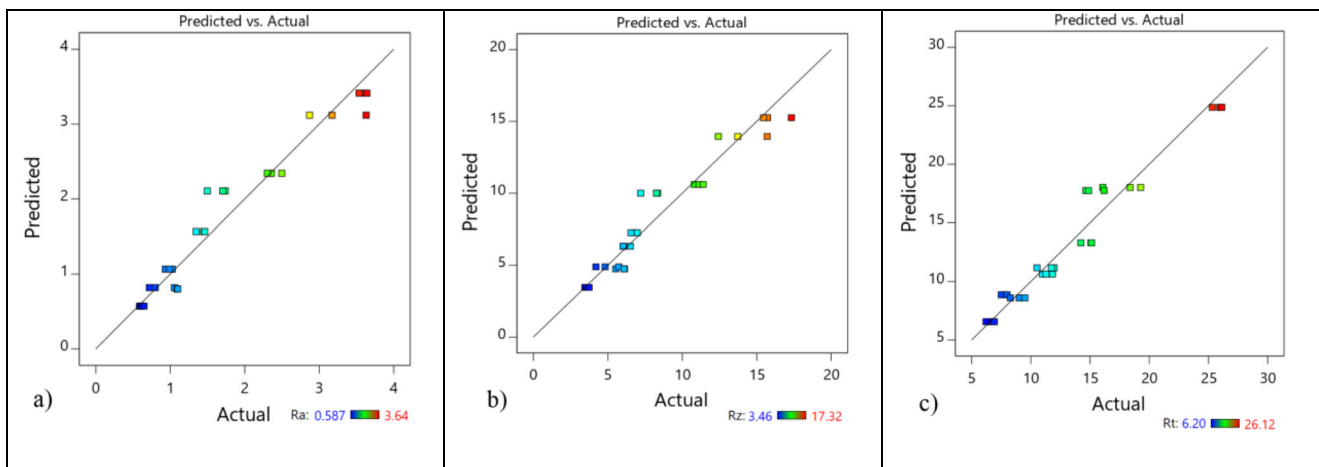


Fig. 13 Regression predictions versus experimental measurements. a R_a roughness. b R_z roughness. c R_t roughness

section. The results are graphically illustrated through 2D contours, 3D surfaces, and curves.

6.1 Effect of forming parameters on axial forces

At feed rate and rolling ball diameter fixed, the average axial force increases simultaneously with step down. Its parabolic

appearance shows in Fig. 17a, c that it tends towards a maximum when step down level exceeds 1 mm. By setting the tool feed rate and step down at fixed levels, the evolution of the average axial force as a function of the rolling ball diameter becomes linear, as per Fig. 17d, f. In general terms, the analysis of the obtained results shows that the average axial forming force is slightly sensitive to the tool feed rate but

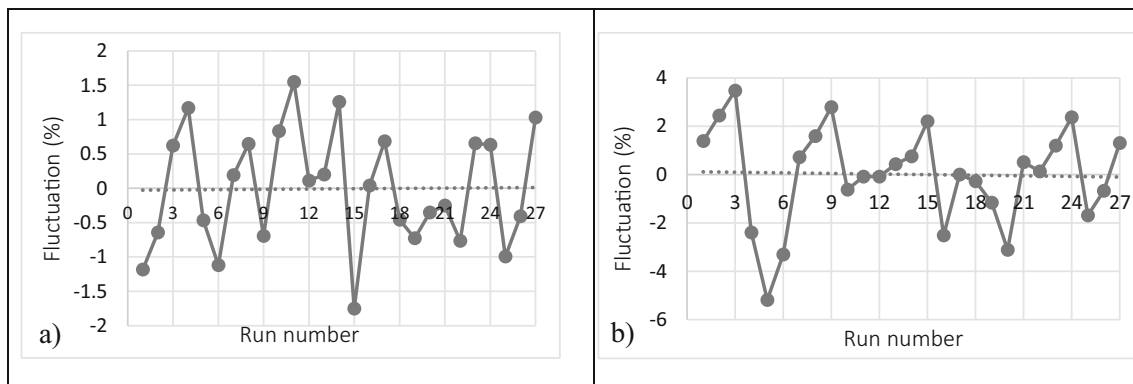


Fig. 14 Axial force fluctuations (%) vs test run number. a F_{avr} . b F_{max}

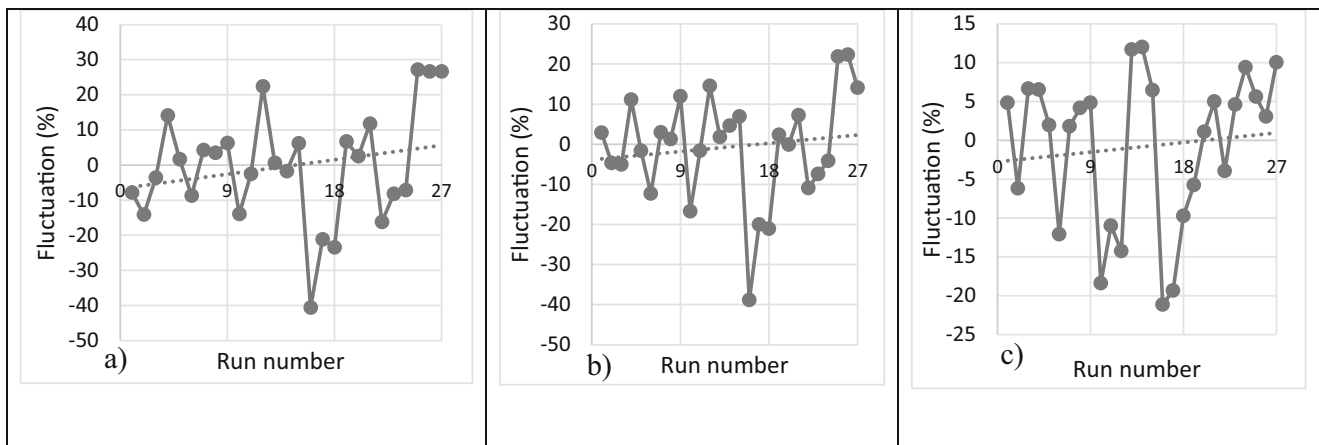


Fig. 15 Surface roughness fluctuations (%) vs test run number. a R_a . b R_z . c R_t

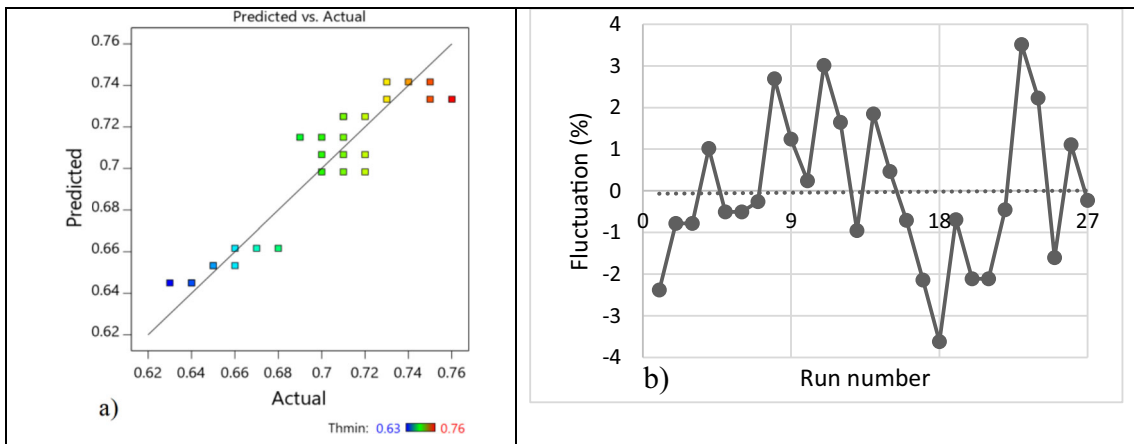


Fig. 16 Thinning distribution. a Regression predictions versus experimental measurements. b Thinning fluctuation (%) vs test run number

highly sensitive to the step down and the rolling ball diameter as shown in Fig. 17a, d.

It should also be noted that the observations and the obtained results confirm that the adequate combination of forming

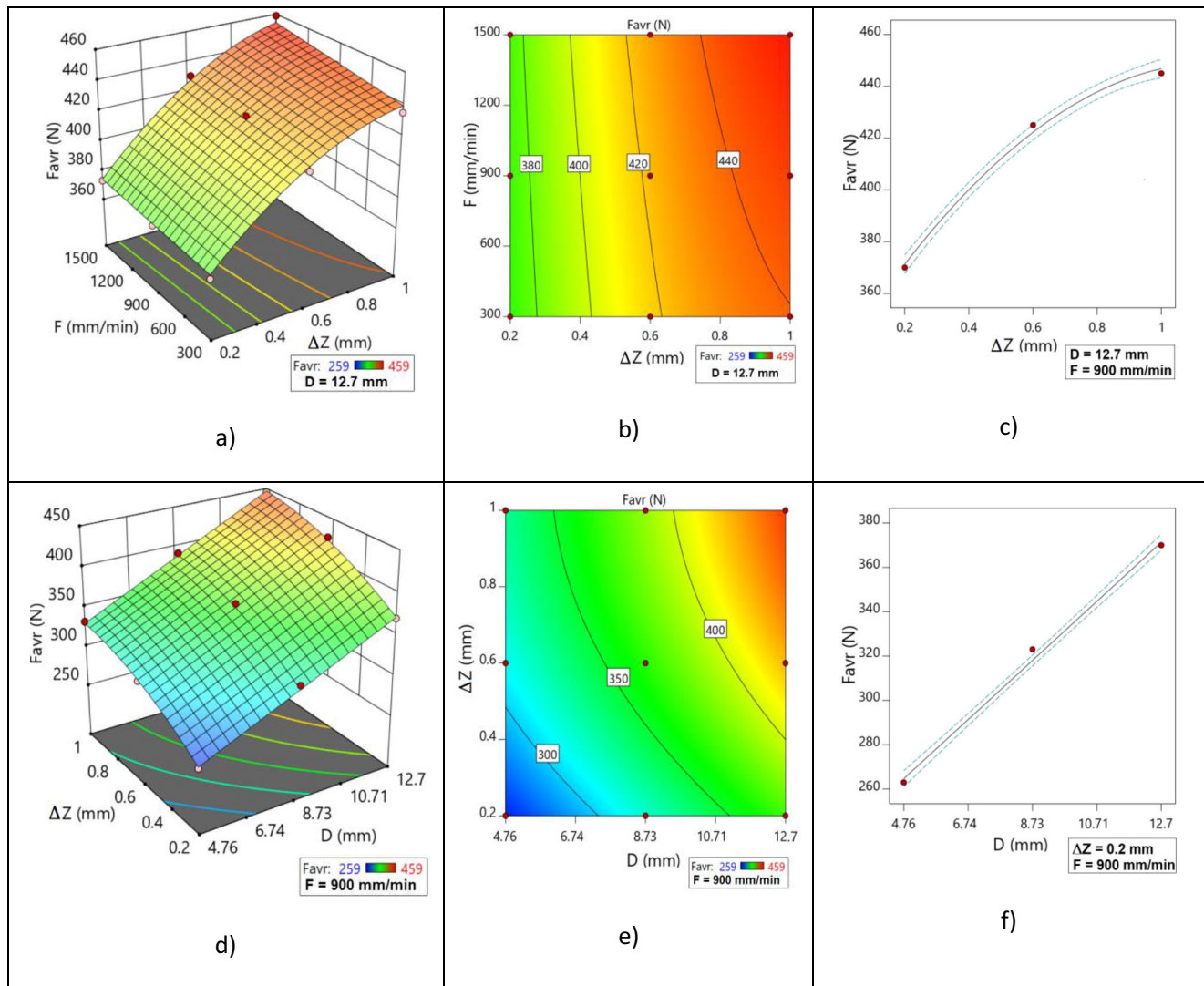


Fig. 17 Effect of the step down and diameter of the rolling ball on the average axial forming force. a 3D surface response F_{avr} vs $(F, \Delta Z)$. b 2D diagram contour F_{avr} vs $(F, \Delta Z)$. c F_{avr} vs step down. d 3D surface response F_{avr} vs $(D, \Delta Z)$. e 2D diagram contour F_{avr} vs $(D, \Delta Z)$. f F_{avr} vs ball diameter

parameters achieve an average axial force of less than 400 N. This limit corresponds to a forming step down ΔZ belonging to the interval [0.2 mm, 0.4 mm] and a ball diameter D between 4.5 mm and 12 mm. The insensitivity of the axial force regarding the variation of the feed rate makes it possible to maintain the latter process parameter in a wide range from 300 to 1500 mm/min. These observations suggest that the optimization of the axial force cannot be done and should not be based only on the forming parameters. Indeed, it is interesting to study the energy impact of the forming parameters in order to validate the obtained result related to the force. Finally, it should be noted that the findings and remarks of the average axial force also could be applied to the maximum axial force with the exception of the feed rate of the tool, which has no influence on it.

6.2 Effect of forming parameters on surface roughness

As the roughness R_a and R_z are insensitive to the feed rate of the forming tool, the most important parameters that affect these responses are the increment and the rolling ball diameter. This finding matches well with what has been obtained in [24, 32], that higher tool diameter values and increment have positive effects on the roughness of the parts. Figure 18a and d illustrate the effects of forming parameters on surface roughness evolution for feed rate equals to 900 mm/min. Indeed, at fixed step down, the responses represented by R_a and R_z decrease almost linearly with the increase of the rolling ball diameter D .

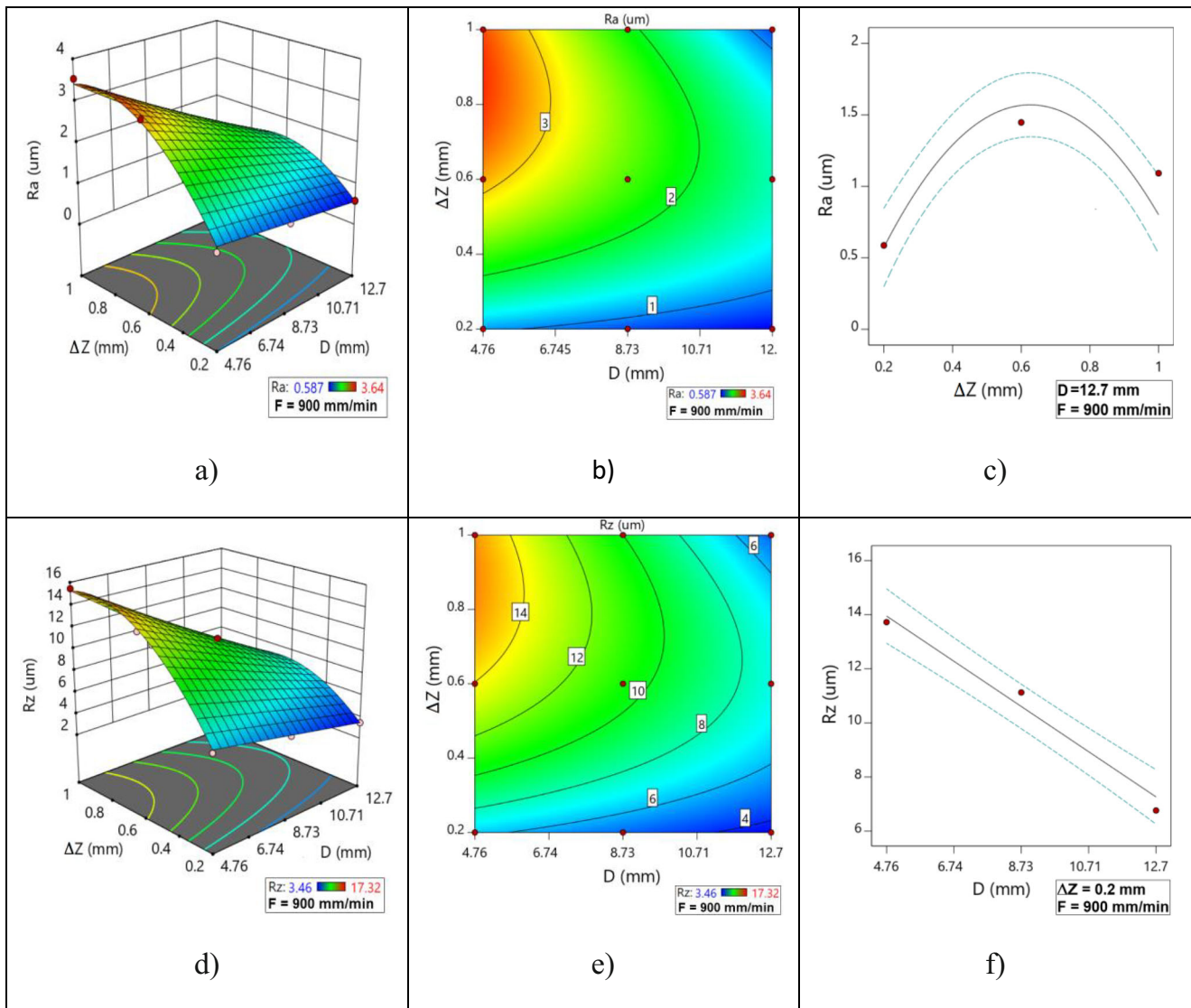


Fig. 18 Effect of forming parameters on surface roughness. **a** 3D surface response R_a vs (D , ΔZ). **b** 2D diagram contour R_a vs (D , ΔZ). **c** R_a vs step down. **d** 3D surface response R_z vs (D , ΔZ). **e** 2D diagram contour (D , ΔZ). **f** R_z vs ball diameter

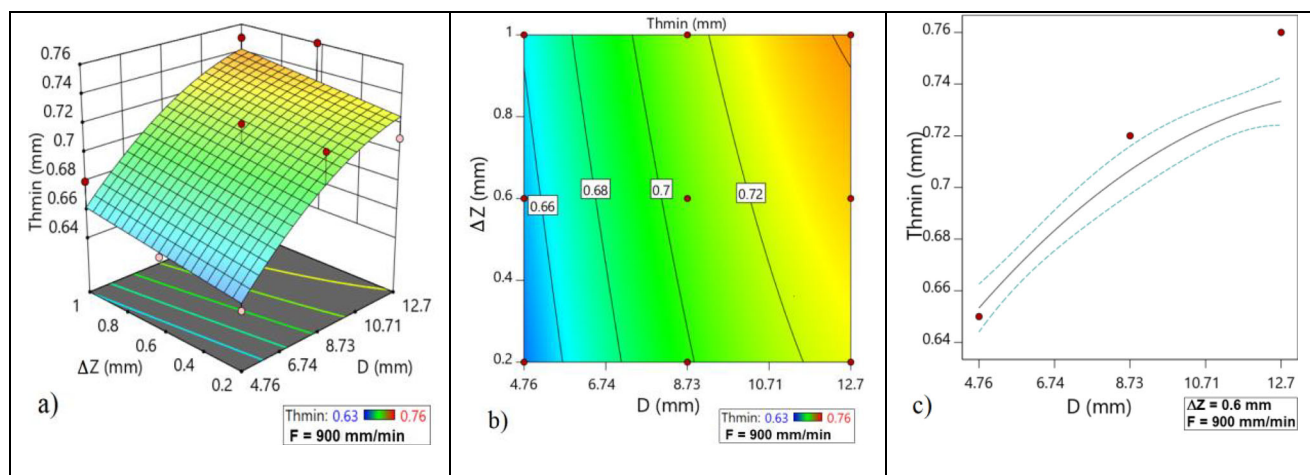


Fig. 19 Effect of forming parameters on sheet thinning. **a** 3D surface response Th_{min} vs (Z, D). **b** 2D diagram contour Th_{min} vs (Z, D). **c** Thinning vs ball diameter

With a fixed ball diameter (here, $D = 12.7$ mm), the evolution of roughness as a function of the increment is characterized by a parabolic rate; the maximums of R_a and R_z are dependent on D and correspond to increment values between 0.6 and 0.8 mm.

The lowest roughness area R_a is to the right of the contour with 1.0 as iso-value (Fig 18b). Two configurations are available to the operator: The first is obtained with conditions $8.5 \text{ mm} < D < 12 \text{ mm}$ and $0.20 \text{ mm} < \Delta Z < 0.30 \text{ mm}$. The second is also obtained with conditions $11 \text{ mm} < D < 12 \text{ mm}$ and $0.95 \text{ mm} < \Delta Z < 1.00 \text{ mm}$. If the operator uses either of these two configurations, he will guarantee the production of finished parts with a surface roughness R_z less than $6 \mu\text{m}$.

6.3 Effect of forming parameters on sheet thinning

The localized weakening of a finished sheet thickness obtained by incremental forming is a potential indicator of the areas where plastic instability is likely to occur. In order to estimate the critical sheet thinning, the operator using the results for the Th_{min} response surface or contour diagram should know the forming limits of the sheet proposed for a forming operation. The results of the analysis developed should facilitate to the operator a justified choice of forming parameters to push the sheet towards its forming limits, without creation of sheet instability zones. In this study, none of the 27 tests led to the cracking of shaped parts; the results obtained (Fig. 19) show that all configurations of forming parameters minimizing axial force and surface roughness can be adopted.

7 Conclusion

The work presented in this paper is focused on the studding of single-point incremental forming process (SPIF). The research work conducted concerns particularly the action of forming

tools with rolling balls on sheets. For that, a preliminary experimental design study was carried out in order to compare two types of forming tools. The first one is a rigid tool with a hemispherical tip. The second one is an invented new tool with a spherical rolling element (Bearing extracted ball) with same diameter as hemispherical end. The experimental results obtained are in favor of tools with spherical rolling elements which generate sheet surfaces of much higher quality, even without lubricant, compared to those obtained with rigid hemispherical end tools. Based on the obtained results, it is observed that with same step down, feed rate, and ball diameter, the forming tests with both types of tools led to axial forces that were quite similar in terms of both aspects and magnitudes. Motivated by the advantage of forming tools with rolling balls improving the generated surface state, an experimental design was performed. Thus, a complete experimental design built with three factors and three levels for each factor was adopted. The analysis is focused on the effects of step down ΔZ , rolling ball diameter D , and feed rate F of the forming tool on the responses expressed in terms of axial forces F_{avr} and F_{max} ; surface roughness R_a , R_z and R_t ; and sheet minimal thinning Th_{min} .

The analysis of experimental results, conducted with Design Expert software, made it possible to establish, using the multiple regression method, predictive analytical models for the different responses. The highest determination coefficient is located at 0.997. It refers to the predictive analytical models of mean and maximum axial forces. The predictive analytical models of the surface roughness generated by SPIF process are obtained with determination coefficients ranging from 0.941 to 0.949. The lowest determination coefficient is assigned to the predictive model (Eq. 7) of the minimum thinning which stands at 0.882. By introducing the percent fluctuation (Eq. 8), a confrontation between experimental results and model predictions could be conducted. Expressed in absolute values, the smallest fluctuations are associated

with the axial forces F_{avr} and F_{max} and evolve from 1.54 to 5.20%, followed by those associated with the sheet minimum thinning Th_{min} , which evolves between 3.47 and 5.19%. The most important fluctuations are recorded for surface roughness and vary from 12.01 to 40.61%.

Finally, it is underlined that the spatial representations of the response surfaces as well as the plane representation contours are largely useful. Indeed, these are largely useful to provide a global view of the responses by highlighting the cumulative effects of the forming process parameters. Their quadratic terms and their interactions, the plotted results show that the different responses collected are slightly sensitive to feed rate F . This is explained by the significant reduction in sliding friction effects at the level of tool/sheet contact. Consequently, the use of a tool equipped with spherical rolling elements can only preserve the integrity of the running surface.

Potentially, this experimental research work can feed a numerical based finite element model that can help to make more physical comprehension accompanying the tool/sheet interaction.

References

- Leszak E (1967) Apparatus and process for incremental dieless forming, United States Patent Office. Patent [US 3342051]
- Mason B, Appleton E (1984) Sheet metal forming for small batches using sacrificial tooling.. In: Proc 3rd Int. Conf. On rotary metal-working, Kyoto, Japan, pp. 495–511
- Emmens WC, Sebastiani G, Boogaard AH (2010) The technology of incremental sheet forming – a brief review of the history. *J Mater Process Technol* 210:981–997
- Iseki H, Kato K, Sakamoto S (1989) Flexible and incremental sheet metal forming using a spherical roller. *Proceedings of 40th JJCTP41–44*
- Matsubara S (1994) Incremental backward bulge forming of a sheet metal with a hemispherical head tool. *J Jpn Soc Technol Plast* 35(1994):1311–1316
- Jeswiet J, Micari F, Hirt G, Bramley A, Dufloy A, Allwood J (2005) Asymmetric single point incremental forming of sheet metal. *CIRP Ann* 54(2):623–649
- Gunashekar G, Kishore K (2017) Modeling and manufacturing of an aerospace component by single point incremental forming process. *International Research Journal of Engineering and Technology* 4(9): 600–603
- Hussain G, Khan HR, Gao L, Hayat N (2013) Guidelines for tool-size selection for single-point incremental forming of an aerospace alloy. *Mater Manuf Process* 28(3):324–329
- Boulila A, Ayadi M, Marzouki S, Slim B (2018) Contribution to a biomedical component production using incremental sheet forming. *Int J Adv Manuf Technol* 95:2821
- Wulf WA (2007) Changes in innovation ecology. *Science* 316:1253
- Behera A K, Alves de Sousa R, Ingarao G, Oleksik V (2017) Single point incremental forming: an assessment of the progress and technology trends from 2005 to 2015. *The Society of Manufacturing Engineers*.1526–6125/2017
- Li Y, Chen X, Liu Z, Sun J, Li F, Li J, Zhao GA Review on the recent development of incremental sheet-forming process. *Int J Adv Manuf Technol* 92:2439–2462
- Bahloul R, Arfa H, BelHadjSalah H (2014) A study on optimal design of process parameters in single point incremental forming of sheet metal by combining Box–Behnken design of experiments, response surface methods and genetic algorithms. *Int J Adv Manuf Technol* 74:163–185
- Gatea S, Ou H, McCartney G (2016) Review on the influence of process parameter in incremental sheet forming. *Int J Adv Manuf Technol* 87:479–499
- Cawley B, Adams D, Jeswiet J (2012) Examining tool shapes in single point incremental forming. *Proc NAMRI/SME* 13(17):163
- Hussain G (2014) Experimental investigations on the role of tool size in causing and controlling defects in single point incremental forming process. *Proc IMechE Part B* 228:266–277
- Siddiqi MUR, Corney JR, Sivaswamy G, Amir M, Bhattacharya R (2017) Design and validation of a fixture for positive incremental sheet forming. *Proc Inst Mech Eng B J Eng Manuf* 232(4):629–643
- Do VC, Lee BH, Yang SH, Kim YS (2017) The forming characteristic in the single-point incremental forming of a complex shape. *Int J Nanomanuf* 13(1):33
- Fernandez C, Trujillo A, Rivero A, Alvarez M, Puerta F J, Salguero J, Marcos M (2016) Implementing incremental sheet metal forming on a CNC machining centre. *Proceedings of the 26th DAAAM International Symposium*, pp.0926–0929, B
- Li Y, Lu H, Daniel WJT, Meehan PA (2015) Investigation and optimization of deformation energy and geometric accuracy in the incremental sheet forming process using response surface methodology. *Int J Adv Manuf Technol* 79:2041–2055
- Ambrogio G, Dufloy J.R, Filice L, Aereus R (2007) Some considerations on force trends in Incremental Forming of different materials. 10th ESAFORM conference on material forming, AIP Conference Proceedings, vol 907, pp 193–198
- Aereus R, Eyckens P, Van Bael A, Dufloy JR (2010) Force prediction for single point incremental forming deduced from experimental and FEM observations. *Int J Adv Manuf Technol* 46:969–982
- Dwivedy M, Kalluri V (2019) The effect of process parameters on forming forces in single point incremental forming. *Procedia Manuf* 29/120–128
- Saidi B, Giraud-Moreau L, Boulila A, Cherouat A, Nasri R (2017) Experimental and numerical study on force reduction in SPIF by using response surface. *Lecture Notes in Mechanical Engineering*, 835–844
- Dufloy JR, Tunçkol Y, Aereus R (2007) Force analysis for single point incremental forming. *Key Eng Mater*:344/543–344/550
- Dufloy J, Tunckol Y, Szekeres A, Vanherck P (2007) Experimental study on force measurements for single point incremental forming. *J Mater Process Technol* 189:65–72
- Liu Z, Liu S, Li Y, Meehan PA (2014) Modeling and optimization of surface roughness in incremental sheet forming using a multi-objective function. *Mater Manuf Process* 29(7):808–818
- Kurra S, Rahman NH, Regalla SP, Gupta AK (2018) Modeling and optimization of surface roughness in single point incremental forming process. *J Mater Res Technol* 4(3):304–313
- Durante M, Formisano A, Langella A, Capece Minutolo FM (2009) The influence of tool rotation on an incremental forming process. *J Mater Process Technol* 209(9):4621–4626
- Durante M, Formisano A, Langella A (2010) Comparison between analytical and experimental roughness values of components created by incremental forming. *J Mater Process Technol* 210(14):1934–1941
- Salem E, Shin J, Nath M, Banu M, Taub A (2016) Investigation of thickness variation in single point incremental forming. *Procedia Manuf*:5/828–5/837

32. Li JC, Li C, Zhou TG (2012) Thickness distribution and mechanical property of sheet metal incremental forming based on numerical simulation. *Trans Nonferrous Metals Soc China* 22(1):58–64
33. Iseki H, Kato K, Sakamoto S (1989) Flexible and incremental sheet metal forming using a spherical roller. *Proceedings of 40th JJCTP*41–44
34. Kim YH, Park JJ (2002) Effect of process parameters on formability in incremental forming of sheet metal. *J Mater Process Technol* 130-131:42–46
35. Shim MS, Park JJ (2001) The formability of aluminum sheet in incremental forming. *J Mater Process Technol* 113(1–3):654–658
36. Matsubara S (2001) Apparatus for dieless forming plate materials, United States Patent Office. Patent [US6216508B1]
37. Zhongyi C (2010) Rolling tool head for incremental forming, Chinese Patent Office. Patent [CN101758135A]
38. Lu B et al (2014) Mechanism investigation of friction-related effects in single point incremental forming using a developed oblique rollerball tool. *Int J Mach Tools Manuf* 85:14–29

Publisher's note Springer Nature remains neutral with regard to jurisdictional claims in published maps and institutional affiliations.